2024 IEEE International Conference on Robotics and Automation (ICRA 2024)
May 13-17, 2024. Yokohama, Japan

Ankle Exoskeleton with a Symmetric 3 DoF Structure for Plantarflexion Assistance

Miha Dežman, Charlotte Marquardt and Tamim Asfour

***Abstract*— Ankle exoskeletons can assist the ankle joint and reduce the metabolic cost of walking. However, many existing ankle exoskeletons constrain the natural 3 degrees of freedom (DoF) of the ankle to limit the exoskeleton's weight and mechanical complexity, thereby compromising comfort and kinematic compatibility with the user.**

This paper presents a novel ankle exoskeleton frame design that allows for 3 DoF ankle motion using a symmetric parallel frame design principle resulting in a strong frame while weighing $1.8\,\mathrm{kg}$. Furthermore, a cable routing method is proposed to actuate the plantarflexion of the ankle. The kinematic compatibility of the proposed exoskeleton frame is evaluated in straight- and curve-walking scenarios with four users. The study demonstrates that the exoskeleton frame adapts to the natural 3 DoF ankle motion and the range of motion (RoM) during walking. The actuation in plantarflexion is evaluated in a stationary torque experiment demonstrating the ability of the frame to transfer large torque loads of up to $57.4\,\mathrm{Nm}$. This work contributes to the design and development of more flexible and adaptable ankle exoskeletons for walking assistance.

I. Introduction

The ankle joint has three degrees of freedom (DoF), supports loads up to four times body weight [1], and provides a large portion of positive power during walking [2]. Exoskeleton devices that assist the ankle joint achieve significant metabolic reductions [3], despite limiting ankle rotation to the sagittal plane. However, exoskeletons should also account for the other two rotations, that is, all three DoF of the ankle, as the ankle moves in all three DoF even during sagittal plane walking [4]. Additionally, an ankle exoskeleton should provide sufficient assistive torque for normal walking. Zhang et al. [5] found that the optimal assistive torque ranged from $0.61\,\mathrm{Nm/kg}$ to $0.85\,\mathrm{Nm/kg}$, which corresponds to an assistive torque of $49\,\mathrm{Nm}$ to $68\,\mathrm{Nm}$ for a $80\,\mathrm{kg}$ user. However, assisting while allowing all three DoF of the ankle increases the mechanical complexity of the device, adds weight, which reduces the benefits of assistance [6].

The kinematic compatibility, i. e., ability to adapt to the posture of a human joint, depends on the adaptability and DoF of a specific exoskeleton frame. An exoskeleton frame is the mechanical interface that holds the exoskeleton components in place and transmits the actuation torque to the cuffs. Fig. 1 shows a comparison of several devices from the literature based on their frame mass and support torque. The devices are grouped into five design principles:

This work has been supported by the Carl Zeiss Foundation through the JuBot project.
The authors are with the High Performance Humanoid Technologies Lab, Institute for Anthropomatics and Robotics, Karlsruhe Institute of Technology (KIT), Germany{miha.dezman,asfour}@kit.edu

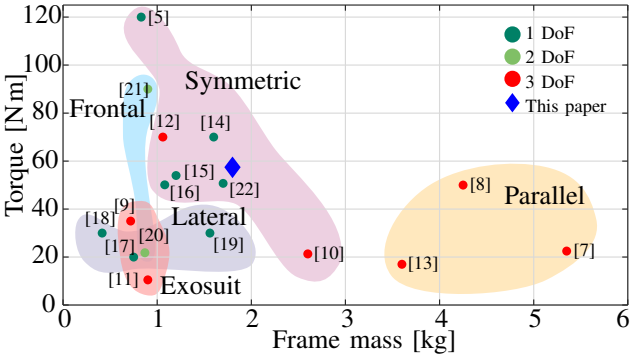

Fig. 1. Ankle exoskeleton design principles and performance classified by their frame design: parallel, symmetric, frontal, lateral, or exosuit. The plot also indicates the number of DoF that each device allows for the ankle joint. The "◆" shows the exoskeleton proposed in this paper.

parallel, symmetric, frontal, lateral and exosuit. The weight and torque performance of an exoskeleton differ according to the frame design principle, making some designs more suitable for reaching higher torques or higher kinematic compatibility while remaining lightweight. In addition, frame designs might have additional features such as direct encoder measurement, weight support, and integrated torque sensing.

Parallel exoskeletons use three linear actuators around the user's leg to actuate all three DoF of the ankle joint [7], [8], [13]. They are used mainly for rehabilitation purposes that require high precision and control [23]. They can produce large torques and feature direct encoder measurement, but are bulky and heavy, which limits their applicability as fully wearable devices.

Frontal exoskeletons use a single linear actuator in front of the shin. These devices are lightweight [20] and can produce large torques [21]. However, this principle does not fully accommodate passive internal/external rotation (IR/ER) of the ankle or feature an integrated angle measurement. Furthermore, the linear actuator pushes the shin cuff upwards, requiring a frontal frame to keep the cuff in place.

Soft exosuit exoskeletons rely on fabric and cables to transfer assistance forces, and are therefore the lightest of the five groups. These devices offer great adaptability to posture and motion [9], [11]. However, they have a low torque capacity that typically does not match the optimal assistance torque range for normal walking. Furthermore, they may not measure ankle angle or joint torque accurately.

Lateral exoskeletons use a rotary actuator at the side of the leg, connecting the foot and shank interface only on one side of the ankle. These devices are lightweight and have a rigid structure [17], [18], [19]. However, the exoskeletons

relying on this asymmetric structure typically feature only 1 DoF and transmit only moderate torques.

Symmetric exoskeletons have a frame design symmetric along the sagittal plane of the leg, with rotation bearings on the lateral and medial sides of the ankle joint [14], [22]. This design reduces the bending forces and allows for a thinner and lighter, yet rigid frame. The lightest 1 DoF exoskeletons in this category weigh between 0.5 kg and 0.6 kg [24], [25] and demonstrate large support torque of up to 120 N m [26]. However, they mostly allow for plantar-/dorsiflexion (PF/DF) movement and sometimes slight in-/eversion (IN/EV) movement [26]. Few devices in this category allow for 3 DoF. An example of such an exoskeleton with 3 DoF is by Weerasingha et al. [10]. This exoskeleton actuates all three DoF and features direct angle measurement, however it does not reach full assistance torques and is one of the heaviest in this category. An important example is the device of Mooney et al. [12]. This design uses two struts connected to a hiking boot to transmit the torques for assistance in plantarflexion (PF). The actuator is placed on the shin. The hiking boot allows some level of IN/EV and IR/ER motion, but the actual DoF is not specified. However, it lacks a rigid connection between the struts and the shank cuff, making it difficult to accurately measure the assistance torque and the joint angles.

This analysis shows that symmetric frame designs achieve the highest torques while remaining lightweight. However, none of the existing devices in the literature combine the following features: 1) a symmetric structure to build a strong and lightweight frame, 2) an actuation method capable of reaching the optimal assistive torque, 3) sufficient DoF and RoM for the ankle joint, and 4) direct measurement of joint torque and absolute joint angle. This paper proposes an exoskeleton that meets these requirements.

The novel frame design and exoskeleton implementing it are intended to assist the elderly and/or healthy individuals who have at least basic motor functions. The inspiration comes from our previous work [27], where a double rod system was used to follow the rotation of the supination/pronation of the lower arm. The new frame design combines this lower arm mechanism with several passive DoF to allow for all three ankle rotations (3 DoF) with additional adjustable passive DoF for adaptability to different shoes and leg sizes. A cable routing method is presented to actuate the PF motion that can reach the optimal assistive torques. A mathematical model is derived to calculate the 3 DoF of the ankle based on the Motion Capture (MOCAP) data. This model is then used to evaluate the effect of the exoskeleton on the user's ankle kinematics in a user-oriented study, focusing on straight and curve walking. Finally, the torque capabilities are evaluated using a stationary experimental setup.

The rest of the paper is organized as follows. Section II introduces the new exoskeleton design and its actuation method. Section III describes the user study and the data analysis methods. Section IV reports and analyzes the results of the user study. Section V discusses the implications, limitations, and future work of this paper. Section VI concludes the paper. Explanations on how to calculate ankle angles from the MOCAP data are in the Appendix.

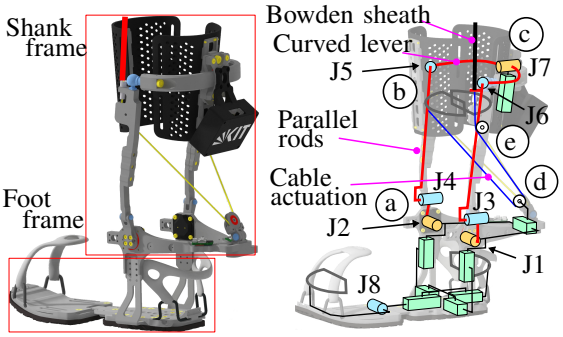

Fig. 2. Exoskeleton shown *left* and the kinematic representation shown *right*. The structure consists of several passive joints: "▭" 1 rotation DoF joint, "○" 3 DoF ball joint, "▭" 1 rotation DoF with an encoder and "▭" 1 DoF adjustable translation joint.

II. Exoskeleton Design

This section describes the new frame design, the exoskeleton that implements it, and the actuation method.

A. Frame design

The ankle exoskeleton is shown in Fig. 2(left), consisting of two main parts: the *Shank* frame and the *Foot* frame.

The *Shank* frame features a novel kinematic structure that adapts to a user's ankle rotations. It has 11 DoF, including several passive 1 DoF joints and two passive 3 DoF joints, as shown in Fig. 2(right). Further features of the *Shank* frame are the following: two cylindrical joints on each side of the exoskeleton (J1, J2, J3, J4), as denoted in Fig. 2 ⓐ, are misaligned for compact integration of the magnetic encoder. The two ball joints (J5, J6) connect each parallel strut to the curved lever, as indicated in Fig. 2 ⓑ, enabling IN/EV and IR/ER of the ankle. A cylindrical joint (J7) connects the curved lever to the exoskeleton cuff, as indicated in Fig. 2 ⓒ, and also features the third encoder. In all, three of the passive joints (J1, J2, J7) feature an integrated absolute encoder (RMB20, RLS d.o.o.) to infer the ankle joint angles.

This passive joint arrangement allows for all three ankle rotations, as demonstrated in Fig. 3. Rotating joints J1 and J2 in the same direction enables PF/DF motion. The rotation of joints J3 and J4, in combination with joints J5 to J7, enables the IN/EV motion. Opposite rotation of joints J1 and J2, in combination with joints J5 to J7, enables the IR/ER.

The current *Foot* frame design is rigid with one passive DoF for rotation of the forefoot, and several adjustable DoF to fit different shoe sizes. The shoe is secured using toe and heel bails adopted from crampons (Petzl, France).

The exoskeleton frame features adaptability in several dimensions both for the *Shank* frame and *Foot* frame, as shown in Fig. 2(right). However, the analysis of these manual adjustments is beyond the scope of this paper.

B. Actuation

The exoskeleton uses a Bowden cable with a Dyneema® rope. The rope is attached to a parallel strut (Fig. 2 ⓑ), routed through a pulley at the end of the foot frame lever

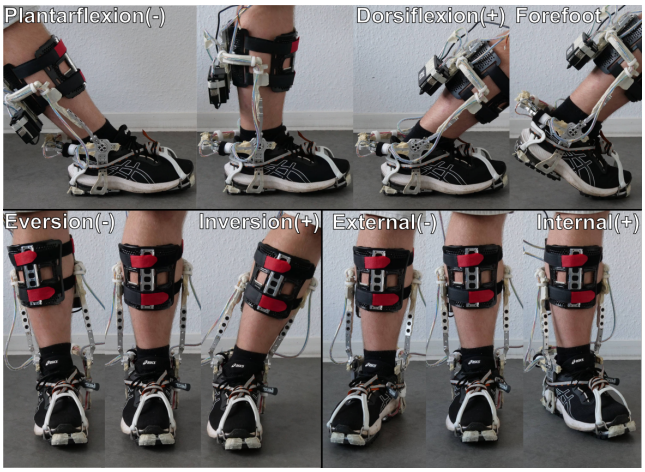

Fig. 3. The proposed exoskeleton kinematics allows PF/DF ($\alpha_{\text{PF/DF}}$), IN/EV ($\alpha_{\text{IN/EV}}$) and IR/ER ($\alpha_{\text{IR/ER}}$) of the ankle joint.

(Fig. 2 ⓓ) and routed into a Bowden sheath (Fig. 2 ⓔ). Pulling the cable causes the PF motion of the frame. The exoskeleton does not actuate in the dorsiflexion direction. The Dyneema cables were removed during the study to remove any influence of exoskeleton actuation.

An actuator unit was designed to exert torque on the proposed frame to demonstrate its strength, and provide a baseline for later actuator design. It consists of a 200 W EC60 brushless motor, a 30 N m 12:1 planetary gearbox, and a 90 mm pulley. It uses the power and control circuit from the ARMAR robots group [28] with a 20 A Gold Twitter motor driver (Elmo Motion Control Ltd.). The static torque tests in this work were performed using an open-loop current controller. In the future, integrated torque sensing will be used to design a closed-loop torque control.

III. Materials and Methods

This section details the user study, joint angle calculation, task segmentation, and static joint torque experiment.

A. User-study

The user study evaluates the effect the exoskeleton has on the ankle angles of the user. In the study, the exoskeleton was used passively without actuation. Four healthy participants (three male, one female) participated in the study. Their information is summarized in Table I. The experiment protocol

TABLE I

Participant information

Height [cm]	Weight [kg]	EU shoe size	Age [y]
176.0 (10.2)	68.8 (6.1)	41.5 (1.7)	26.0 (3.6)
165-187	63-75	40-43	23-31

Values represent the mean, standard deviation and range.

was approved by the Karlsruhe Institute of Technology (KIT) Ethics Committee under the JuBot project. All participants provided written informed consent before the experiment.

The participants performed two tasks: 1) *walk normal*, where they walked along a straight path and turned around twice, and 2) *walk eight*, where they walked on a path shaped like an eight, similar to slalom walking. The two conditions were; *withExo* and *noExo*. The tasks were designed to test the three rotations of the ankle: PF/DF, IN/EV, and IR/ER. The dimensions of the path were as large as possible while still allowing for continuous MOCAP.

Before the study, the *Foot* frame was adjusted based on the participant's shoe size. During the donning process, the exoskeleton was aligned so that the ankle axis coincides with the location of the user's medial malleolus. During the study, the motion of both the exoskeleton and the participant were captured independently by an optical motion capture system (Vicon Motion System, Ltd, UK). Passive markers were attached to the exoskeleton and participant in a way that all three rotations of the ankle joint can be tracked in both conditions, as shown in Fig. 4.

B. Joint Angle Calculation

The leg markers were placed for easier vector based calculation of the ankle joint angles (see Appendix). Figure 4(left) shows the markers and Fig. 4(right) shows the shank and foot axes derived from them. The three ankle motions, PF/DF ($\alpha_{\text{PF/DF}}$), IN/EV ($\alpha_{\text{IN/EV}}$), and internal/external ($\alpha_{\text{IR/ER}}$), are demonstrated in Fig. 3.

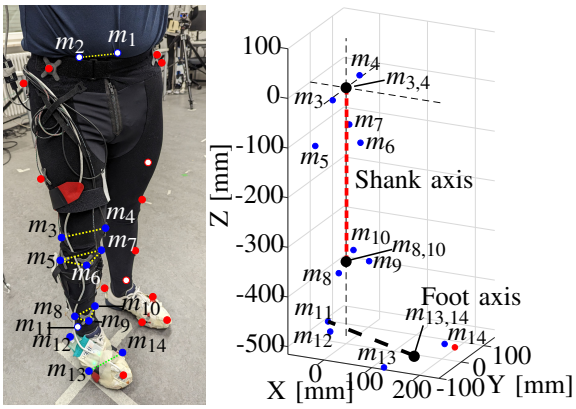

Fig. 4. Participant with markers (left) and a 3D plot of calculated shank and foot axes (right) using markers depicted in blue.

C. Task Segmentation and Analysis

The raw angle data was first segmented based on the heel switch activation to remove all transient strides. Next, the orientation of markers m_1 and m_2 was used to extract the turning direction of the participants in the *walk eight* task, where $v_{\text{B}} = \vec{m}_2 - \vec{m}_1$. This allows classification of the strides based on the user rotation direction. The markers m_1 and m_2 were first centered at the origin using their midpoint $m_{1,2}$. Absolute rotation θ in the room was calculated with atan2 and unwrap functions with MATLAB®. The absolute angular velocity ω is the derivative of θ. It follows that:

$$\theta = \text{unwrap}(\text{atan2}(v_{\text{B,y}}, v_{\text{B,x}})) + \pi/2, \quad (1) \quad \omega = \frac{\text{d}}{\text{d}t}\theta. \quad (2)$$

The walking direction of each MOCAP recording was classified using ω with an empirically chosen threshold, as in Fig. 5(left). The segmented path is shown in Fig. 5(right). This classifies stride according to the angular velocity, where

$\omega = 0$ means walking straight, $\omega > 0$ means turning left, and $\omega < 0$ means turning right. Once all of the strides are

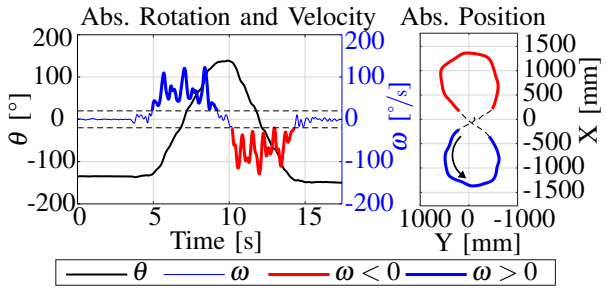

Fig. 5. Participant's θ angle and ω derivative (left) and position and orientation in the room (right). The arrow shows the direction of travel. Blue areas walking left: $\omega > 0$. Red areas walking right: $\omega < 0$.

classified, mean and standard deviation of all strides of all participant are calculated.

The change in the joint angle trajectories of the motion with the exoskeleton (*withExo*) relative to the motion without the exoskeleton (*noExo*) were calculated as the root-mean-squared error (RMSE) difference between these signal averages. A lower RMSE value corresponds to the joint angle trajectory being more similar to the baseline signal.

Furthermore, the RoM for all conditions and tasks was calculated by taking the maximum and minimum values of the mean angle and its standard deviation.

D. Joint Torque Measurement

Nominal and peak joint torque was measured in a stationary setup restricted to only one DoF, the PF/DF of the ankle, as shown in Fig. 6. The objective of this experiment was to test the strength of the exoskeleton design and determine the maximum actuation torque. The effect of the exoskeleton actuation on the user is not evaluated at this stage, but will be thoroughly investigated in the future.

In the experiment, the exoskeleton pulled on a load cell (500N DCE, LCM Systems Ltd.) while in the neutral frame rotation ($\alpha_{\text{PF/DF}} = 0°$). The joint torque was derived from the reading of the load cell assuming a lever of 133 mm. The exoskeleton frame was actuated by a sequence of step signals with two different currents in a feedforward manner: 9.28 A (nominal motor current) and 19.5 A (maximum motor driver current). The current was increased from a starting 3 A to ensure the rope stays tensioned. After the experiment, the mean and standard deviation of the torque, current and power were calculated. The resulting torque, i. e., joint torque, represents the torque the exoskeleton would exert on the user's joint.

IV. Results and Analysis

This section presents the results of the user study and stationary torque measurements.

A. Joint Angles

The ankle joint angles for different tasks and conditions are collected in Fig. 7. The columns depict the three angles, that is, PF/DF ($\alpha_{\text{PF/DF}}$), IN/EV ($\alpha_{\text{IN/EV}}$), and IR/ER ($\alpha_{\text{IR/ER}}$).

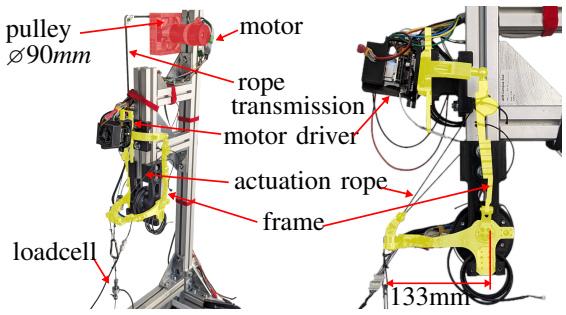

Fig. 6. Stationary experimental setup for evaluations of joint torque.

The rows represent the three tasks, that is, walking straight ($\omega = 0$), turning left ($\omega > 0$), and turning right ($\omega < 0$). The red curves correspond to the *noExo* condition and the blue curve to the *withExo* condition.

The results demonstrate that the exoskeleton follows the 3 DoF motions of the ankle, since the joint angles are similar under all conditions. This is denoted by the similarity between the red and blue curves and confirmed by the small RMSE values. There are some subtle differences and phase shifts between the curves, attributed to the rigid sole.

Figure 8 shows how turning affects RoM of the ankle. When participants start the turning motion, the angles and RoM change, especially $\alpha_{\text{IN/EV}}$ and $\alpha_{\text{IR/ER}}$. The RoM is affected by the walking direction, especially for IN/EV and IR/ER. Turning to the left or right causes a change in the sign and magnitude of the RoM for these angles. The RoM for PF/DF is less affected by the turning direction. In all conditions, the ankle RoM is similar between the *withExo* case and *noExo* case, again demonstrating the kinematic compatibility of the exoskeleton.

B. Joint Torque measurement

Figure 9 displays the results of the torque experiment, with Fig. 9(left) showing the resulting nominal and maximum PF joint torque. Figure 9(right) shows the nominal and maximum target current sent to the motor.

The proposed ankle exoskeleton can reach a nominal joint torque of 26.8 N m and a maximum joint torque of 57.4 N m. The actuator setup can reach a maximum power output of 491 W. The oscillations observed in Fig. 9(left) are the consequence of the open-loop control and the elasticity in the aluminium construction elements of the experimental setup.

V. Discussion

The similar ankle trajectories demonstrate the exoskeleton's ability to follow the RoM of the ankle. However, the shape of the angle curves was not unaffected. The rigid exoskeleton sole is considered as one of the causes. It enables a secure attachment of the exoskeleton to the shoe, however, its rigidity may be the cause for the phase delays observed in PF/DF from Fig. 7. This is supported by the results of a previous study in the literature, where rigid soled shoes were shown to cause similar effects [29]. However, no literature was found to confirm the same for curved walking. Although participants felt comfortable with the

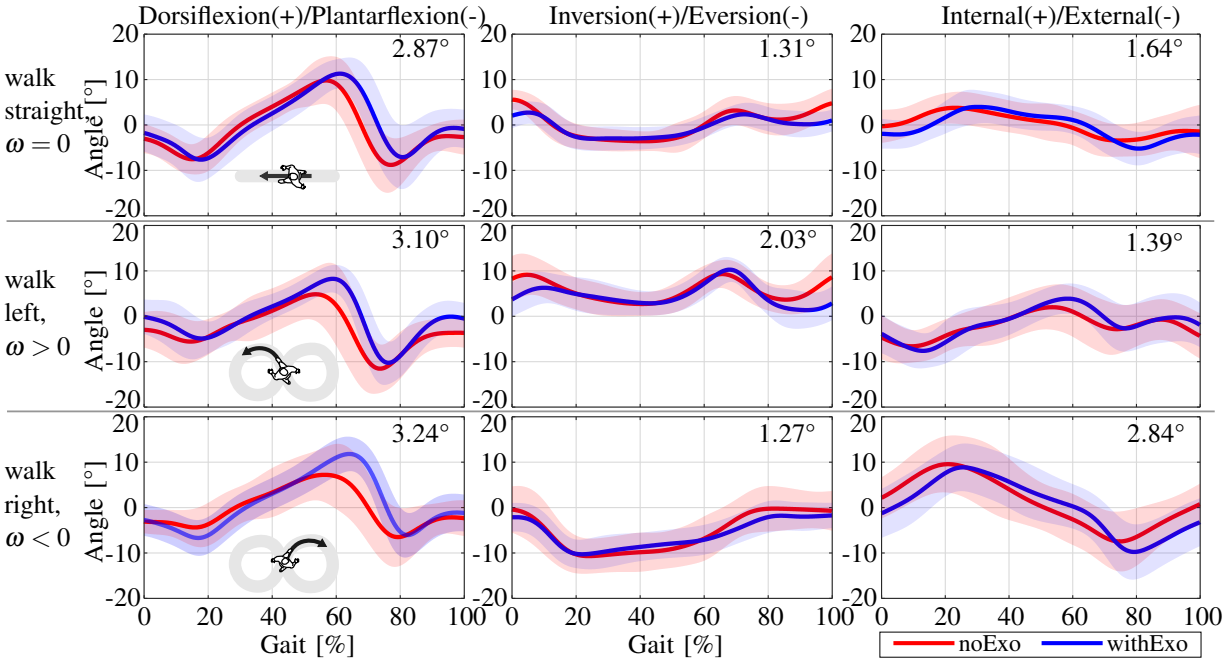

Fig. 7. The average ankle angle for the *noExo* (red) and for the *withExo* condition (blue). The columns show the three ankle rotations: PF/DF, IN/EV, and IR/ER. The rows show the three walking directions: straight ($\omega = 0$), left ($\omega > 0$) and right ($\omega < 0$). The shaded areas show the standard deviation of all collected strides from all participants. The black numbers show the RMSE as the difference between the *withExo* and *noExo* condition.

exoskeleton, they reported exoskeleton weight as a significant disadvantage. Therefore, a lighter *Foot* frame and sole design will be the first priority for improvement, thus reducing the weight of the exoskeleton. Ultimately, the rigid sole will be removed, following the approach of [26], leading to a better utilization of the shoe's own sole. This will be combined with strength-to-weight optimization of the *Shank* frame.

The device's weight and maximum torque position the proposed device in the middle of the symmetric group in Fig. 1. The device is lighter than all 3 DoF parallel exoskeletons from Fig. 1, and lighter and stronger than the 3 DoF exoskeleton of [10]. The device of Mooney et al. [12] is the only lighter and stronger that features 3 DoF. However, it lacks sensors for accurate measurement of angle and torque. Future strength-to-weight and actuation improvements will position the device closer to the top left corner of Fig. 1.

The static joint torque measurement was restricted to 1 DoF to simplify the experimental setup. In theory, the exoskeleton can provide PF assistance while allowing passive IN/EV and IR/ER of the ankle. However, during the motion, the actuation forces may affect all 3 DoF and act

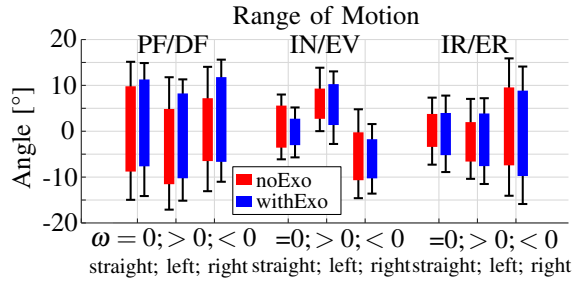

Fig. 8. RoM for the *noExo* (red) and *withExo* (blue) based on maximum and minimum values of Fig. 7. The black lines show standard deviation.

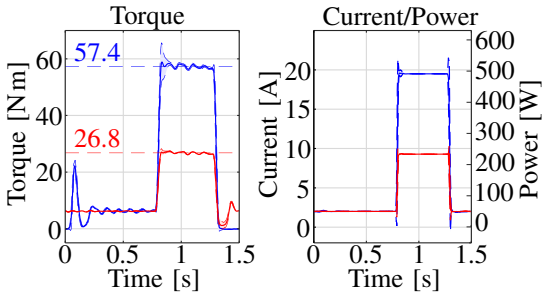

Fig. 9. The nominal (red) and maximal (blue) joint torque shown left, with the corresponding current and power shown right.

asymmetrically to twist the bars in the direction of further rotation. This effect and its implications will be investigated in the future.

VI. Conclusion

This paper introduces a novel 3 DoF ankle exoskeleton with a symmetric frame design that can transmit large torques. The proposed frame design enables new options for design of lightweight ankle exoskeleton devices that may feature 2 DoF or 3 DoF by benefiting from strength advantages of symmetric frame design principles typically used in 1 DoF exoskeletons.

The user study shows that the exoskeleton accomodates the three ankle movement DoF in both straight and curve walking tasks, which have not been extensively explored in previous studies. Furthermore, the actuation experiments demonstrate the strength and robustness of the symmetric frame design. Future work will involve design improvements and weight reductions, implementation of torque control and further investigations through user studies.

APPENDIX

This appendix explains the calculation of the ankle joint angles from the marker coordinates on the leg. Markers can be seen as vectors of origin. For this calculation, only the vector rotations are relevant and not their magnitudes. $\vec{v}_S$ and $\vec{v}_F$ are the shank and foot vectors lying on the shank and foot axes, respectively. $\vec{v}_S$ points from markers $\vec{m}_{8,10}$ to $\vec{m}_{3,4}$ and $\vec{v}_F$ points from markers $\vec{m}_{11}$ to $\vec{m}_{13,14}$:

$$\vec{v}_S = \vec{m}_{3,4} - \vec{m}_{8,10}. \quad (3) \qquad \vec{v}_F = \vec{m}_{13,14} - \vec{m}_{11}. \quad (4)$$

The midpoint vectors $\vec{m}_{3,4}$, $\vec{m}_{8,10}$ and $\vec{m}_{13,14}$ are the averages of the respective markers.

The **plantar-/dorsiflexion** angle $\alpha_{PF/DF}$ is between vectors $\vec{v}_F$ and $\vec{v}_S$, and is calculated as:

$$\alpha_{PF/DF} = \pi/2 - \operatorname{acos}\left(\frac{\vec{v}_F \cdot \vec{v}_S}{|\vec{v}_F||\vec{v}_S|}\right), \quad (5)$$

where $\pi/2$ is added to reflect the neutral position at 90°.

The **in-/eversion** angle $\alpha_{IN/EV}$ describes how markers $\vec{m}_{12}$ and $\vec{m}_{13}$ rotate around vector $\vec{v}_F$. To calculate it, we need a reference vector $\vec{v}_2$ that is perpendicular to $\vec{v}_F$, aligned with $\vec{v}_S$, and obtained by using another vector $\vec{v}_1$ that is orthogonal to both $\vec{v}_F$ and $\vec{v}_S$:

$$\vec{v}_1 = \vec{v}_F \times \vec{v}_S, \quad (6) \qquad \vec{v}_2 = \vec{v}_1 \times \vec{v}_F. \quad (7)$$

Fig. 10(left) shows both vectors in a 3D plot.

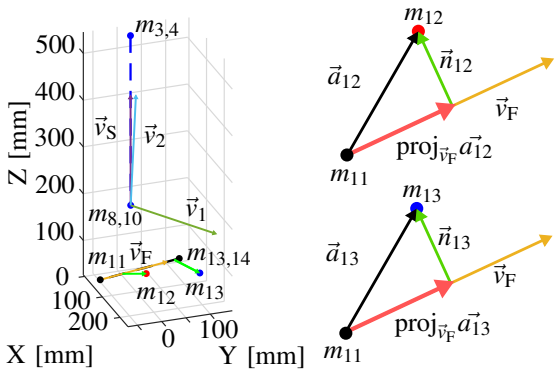

Fig. 10. IN/EV calculation with relevant vectors shown left, and the respective vector projections shown right.

The normal to vector $\vec{v}_F$ is required for both markers $\vec{m}_{12}$ and $\vec{m}_{13}$ to calculate $\alpha_{IN/EV}$. It is obtained through vector projections, as shown in Fig. 10(right). Vectors $\vec{a}_{12}$ and $\vec{a}_{13}$, with their origins at $\vec{m}_{11}$, point at the markers $\vec{m}_{12}$ and $\vec{m}_{13}$, respectively:

$$\vec{a_{12}} = \vec{m}_{12} - \vec{m}_{11}, \quad (8) \qquad \vec{a_{13}} = \vec{m}_{13} - \vec{m}_{11}. \quad (9)$$

Their projections on $\vec{v}_F$:

$$\operatorname{proj}_{\vec{v}_F}\vec{a_{12}} = \frac{\vec{a}_{12} \cdot \vec{v}_F}{\vec{v}_F \cdot \vec{v}_F}\vec{v}_F, \quad (10) \qquad \operatorname{proj}_{\vec{v}_F}\vec{a_{13}} = \frac{\vec{a}_{13} \cdot \vec{v}_F}{\vec{v}_F \cdot \vec{v}_F}\vec{v}_F \quad (11)$$

lead to the normal vectors (as in Fig. 10(right)):

$$\vec{n}_{12} = \vec{a_{12}} - \operatorname{proj}_{\vec{v}_F}\vec{a_{12}}, \quad (12) \qquad \vec{n}_{13} = \vec{a_{13}} - \operatorname{proj}_{\vec{v}_F}\vec{a_{13}}, \quad (13)$$

which results in the angles

$$\alpha_{IN/EVa} = \operatorname{acos}\left(\frac{\vec{v}_2 \cdot \vec{n}_{12}}{|\vec{v}_2||\vec{n}_{12}|}\right) - \frac{\pi}{2}, \quad (14) \qquad \alpha_{IN/EVb} = \operatorname{acos}\left(\frac{\vec{v}_2 \cdot \vec{n}_{13}}{|\vec{v}_2||\vec{n}_{13}|}\right) - \frac{\pi}{2}. \quad (15)$$

Finally, $\alpha_{IN/EV}$ is the average of both $\alpha_{IN/EVa}$ and $\alpha_{IN/EVb}$:

$$\alpha_{IN/EV} = (\alpha_{IN/EVa} + \alpha_{IN/EVb})/2. \quad (16)$$

The **internal/external rotation** angle $\alpha_{IR/ER}$ measures how vector $\vec{v}_F$ rotates around vector $\vec{v}_S$. $\alpha_{IR/ER}$ is determined through a reference vector based on markers $\vec{m}_5$ and $\vec{m}_7$. Two vectors $\vec{a}_5$ and $\vec{a}_7$ point from $\vec{m}_{8,10}$ to the corresponding marker $\vec{m}_5$ or $\vec{m}_7$:

$$\vec{a}_5 = \vec{m}_5 - \vec{m}_{8,10}, \quad (17) \qquad \vec{a}_7 = \vec{m}_7 - \vec{m}_{8,10}, \quad (18)$$

Fig. 11(left) shows both vectors in a 3D plot.

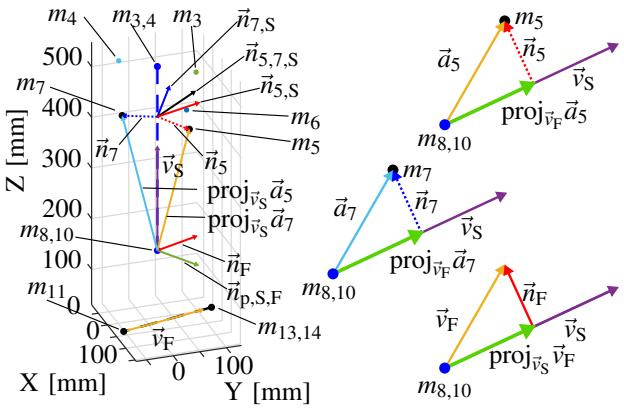

Fig. 11. IR/ER calculation with relevant vectors shown left, and the respective vector projections shown right.

Again, their projections on vector $\vec{v}_S$

$$\operatorname{proj}_{\vec{v}_S}\vec{a}_5 = \frac{\vec{a}_5 \cdot \vec{v}_S}{\vec{v}_S \cdot \vec{v}_S}\vec{v}_S, \quad (19) \qquad \operatorname{proj}_{\vec{v}_S}\vec{a}_7 = \frac{\vec{a}_7 \cdot \vec{v}_S}{\vec{v}_S \cdot \vec{v}_S}\vec{v}_S \quad (20)$$

lead to vectors $\vec{n}_5$ and $\vec{n}_7$, which are normal to $\vec{v}_S$:

$$\vec{n}_5 = \vec{a}_5 - \operatorname{proj}_{\vec{v}_S}\vec{a}_5, \quad (21) \qquad \vec{n}_7 = \vec{a}_7 - \operatorname{proj}_{\vec{v}_S}\vec{a}_7. \quad (22)$$

Their ortogonals to $\vec{v}_S$ are calculated as cross products:

$$\vec{n}_{5,S} = \vec{v}_S \times \vec{n}_5, \quad (23) \qquad \vec{n}_{7,S} = \vec{n}_7 \times \vec{v}_S, \quad (24)$$

and finally averaged to one vector

$$\vec{n}_{5,7,S} = \frac{(\vec{n}_{5,S} + \vec{n}_{7,S})}{2}. \quad (25)$$

Next, $\vec{v}_F$ is projected to $\vec{v}_S$ to calculate $\vec{n}_F$

$$\operatorname{proj}_{\vec{v}_S}\vec{v}_F = \frac{\vec{v}_F \cdot \vec{v}_S}{\vec{v}_S \cdot \vec{v}_S}\vec{v}_S, \quad (26) \qquad \vec{n}_F = \vec{v}_F - \operatorname{proj}_{\vec{v}_S}\vec{v}_F. \quad (27)$$

Vector $\vec{n}_{p,S,F}$ is ortogonal to $\vec{n}_F$ and $\vec{v}_S$ and calculated as:

$$\vec{n}_{p,S,F} = \vec{n}_F \times \vec{v}_S. \quad (28)$$

Finally, $\alpha_{IR/ER}$ is calculated as the angle between vectors $\vec{n}_{p,S,F}$ and $\vec{n}_{5,7,S}$ as:

$$\alpha_{IR/ER} = \operatorname{acos}\left(\frac{\vec{n}_{5,7,S} \cdot \vec{n}_{p,S,F}}{|\vec{n}_{5,7,S}||\vec{n}_{p,S,F}|}\right) - \pi/2, \quad (29)$$

where $\pi/2$ shifts the neutral position for 90°.

REFERENCES

[1] R. P. Kleipool and L. Blankevoort, "The relation between geometry and function of the ankle joint complex: A biomechanical review," *Knee Surgery, Sports Traumatology, Arthroscopy*, vol. 18, no. 5, pp. 618–627, May 2010.

[2] G. S. Sawicki and D. P. Ferris, "Mechanics and energetics of level walking with powered ankle exoskeletons," *Journal of Experimental Biology*, vol. 211, no. 9, pp. 1402–1413, May 2008. [Online]. Available: https://journals.biologists.com/jeb/article/211/9/1402/18202/Mechanics-and-energetics-of-level-walking-with

[3] K. L. Poggensee and S. H. Collins, "How adaptation, training, and customization contribute to benefits from exoskeleton assistance," *Science Robotics*, vol. 6, no. 58, p. eabf1078, Sep. 2021.

[4] J. D. Hsu, J. W. Michael, J. R. Fisk, and American Academy of Orthopaedic Surgeons, Eds., *AAOS Atlas of Orthoses and Assistive Devices*, 4th ed. Philadelphia: Mosby/Elsevier, 2008.

[5] J. Zhang, P. Fiers, K. A. Witte, R. W. Jackson, K. L. Poggensee, C. G. Atkeson, and S. H. Collins, "Human-in-the-loop optimization of exoskeleton assistance during walking," *Science*, vol. 356, no. 6344, pp. 1280–1284, Jun. 2017.

[6] R. C. Browning, J. R. Modica, R. Kram, and A. Goswami, "The effects of adding mass to the legs on the energetics and biomechanics of walking," *Medicine & Science in Sports & Exercise*, vol. 39, no. 3, pp. 515–525, 2007.

[7] A. C. Satici, A. Erdogan, and V. Patoglu, "Design of a reconfigurable ankle rehabilitation robot and its use for the estimation of the ankle impedance," in *2009 IEEE International Conference on Rehabilitation Robotics*. Kyoto, Japan: IEEE, Jun. 2009, pp. 257–264.

[8] A. Erdogan, B. Celebi, A. C. Satici, and V. Patoglu, "Assist On-Ankle: A reconfigurable ankle exoskeleton with series-elastic actuation," *Autonomous Robots*, vol. 41, no. 3, pp. 743–758, Mar. 2017.

[9] S. Lee, J. Kim, L. Baker, A. Long, N. Karavas, N. Menard, I. Galiana, and C. J. Walsh, "Autonomous multi-joint soft exosuit with augmentation-power-based control parameter tuning reduces energy cost of loaded walking," *Journal of NeuroEngineering and Rehabilitation*, vol. 15, no. 1, p. 66, Dec. 2018.

[10] A. Weerasingha, A. Pragnathilaka, W. Withanage, R. Ranaweera, and R. Gopura, "C-JAE: 3 DOF Robotic Ankle Exoskeleton with Compatible Joint Axes," in *2018 Moratuwa Engineering Research Conference (MERCon)*. Moratuwa: IEEE, May 2018, pp. 270–275.

[11] L. N. Awad, J. Bae, K. O'Donnell, S. M. M. De Rossi, K. Hendron, L. H. Sloot, P. Kudzia, S. Allen, K. G. Holt, T. D. Ellis, and C. J. Walsh, "A soft robotic exosuit improves walking in patients after stroke," *Science Translational Medicine*, vol. 9, no. 400, p. eaai9084, Jul. 2017.

[12] L. M. Mooney and H. M. Herr, "Biomechanical walking mechanisms underlying the metabolic reduction caused by an autonomous exoskeleton," *Journal of NeuroEngineering and Rehabilitation*, vol. 13, no. 1, p. 4, Dec. 2016.

[13] A. Roy, H. Krebs, D. Williams, C. Bever, L. Forrester, R. Macko, and N. Hogan, "Robot-Aided Neurorehabilitation: A Novel Robot for Ankle Rehabilitation," *IEEE Transactions on Robotics*, vol. 25, no. 3, pp. 569–582, Jun. 2009.

[14] D. P. Ferris, J. M. Czerniecki, and B. Hannaford, "An Ankle-Foot Orthosis Powered by Artificial Pneumatic Muscles," *Journal of Applied Biomechanics*, vol. 21, no. 2, pp. 189–197, May 2005.

[15] P. Slade, M. J. Kochenderfer, S. L. Delp, and S. H. Collins, "Personalizing exoskeleton assistance while walking in the real world," *Nature*, vol. 610, no. 7931, pp. 277–282, Oct. 2022.

[16] P.-C. Kao, C. L. Lewis, and D. P. Ferris, "Invariant ankle moment patterns when walking with and without a robotic ankle exoskeleton," *Journal of Biomechanics*, vol. 43, no. 2, pp. 203–209, Jan. 2010.

[17] Z. F. Lerner, G. M. Gasparri, M. O. Bair, J. L. Lawson, J. Luque, T. A. Harvey, and A. T. Lerner, "An Untethered Ankle Exoskeleton Improves Walking Economy in a Pilot Study of Individuals With Cerebral Palsy," *IEEE Transactions on Neural Systems and Rehabilitation Engineering*, vol. 26, no. 10, pp. 1985–1993, Oct. 2018.

[18] G. Orekhov, Y. Fang, C. F. Cuddeback, and Z. F. Lerner, "Usability and performance validation of an ultra-lightweight and versatile untethered robotic ankle exoskeleton," *Journal of NeuroEngineering and Rehabilitation*, vol. 18, no. 1, p. 163, Dec. 2021.

[19] J. de Miguel-Fernandez, C. Pescatore, A. Mesa-Garrido, C. Rikhof, E. Prinsen, J. M. Font-Llagunes, and J. Lobo-Prat, "Immediate Biomechanical Effects of Providing Adaptive Assistance With an Ankle Exoskeleton in Individuals After Stroke," *IEEE Robotics and Automation Letters*, vol. 7, no. 3, pp. 7574–7580, Jul. 2022.

[20] H. Choi, Y. J. Park, K. Seo, J. Lee, S.-e. Lee, and Y. Shim, "A Multifunctional Ankle Exoskeleton for Mobility Enhancement of Gait-Impaired Individuals and Seniors," *IEEE Robotics and Automation Letters*, vol. 3, no. 1, pp. 411–418, Jan. 2018.

[21] C. Khazoom, C. Veronneau, J.-P. L. Bigue, J. Grenier, A. Girard, and J.-S. Plante, "Design and Control of a Multifunctional Ankle Exoskeleton Powered by Magnetorheological Actuators to Assist Walking, Jumping, and Landing," *IEEE Robotics and Automation Letters*, vol. 4, no. 3, pp. 3083–3090, Jul. 2019.

[22] D. P. Ferris, K. E. Gordon, G. S. Sawicki, and A. Peethambaran, "An improved powered ankle–foot orthosis using proportional myoelectric control," *Gait & Posture*, vol. 23, no. 4, pp. 425–428, Jun. 2006.

[23] M. G. Alvarez-Perez, M. A. Garcia-Murillo, and J. J. Cervantes-Sánchez, "Robot-assisted ankle rehabilitation: A review," *Disability and Rehabilitation: Assistive Technology*, vol. 15, no. 4, pp. 394–408, May 2020.

[24] S. H. Collins, M. B. Wiggin, and G. S. Sawicki, "Reducing the energy cost of human walking using an unpowered exoskeleton," *Nature*, vol. 522, no. 7555, pp. 212–215, Jun. 2015.

[25] S. Kim, Y. Son, S. Choi, S. Ham, and C. Park, "Design of a simple, lightweight, passive-elastic ankle exoskeleton supporting ankle joint stiffness," *Review of Scientific Instruments*, vol. 86, no. 9, p. 095107, Sep. 2015.

[26] K. A. Witte and S. H. Collins, "Design of Lower-Limb Exoskeletons and Emulator Systems," in *Wearable Robotics*, J. Rosen and P. W. Ferguson, Eds. Elsevier, 2020, pp. 251–274. [Online]. Available: https://www.sciencedirect.com/science/article/pii/B9780128146590000138

[27] *Exoskeleton arm pronation/supination assistance mechanism with a guided double rod system*. IEEE, 2019. [Online]. Available: https://ieeexplore.ieee.org/document/9034992

[28] S. Rader, L. Kaul, P. Weiner, and T. Asfour, "Highly Integrated Sensor-Actuator-Controller Units for Modular Robot Design," in *IEEE International Conference on Advanced Intelligent Mechatronics (AIM)*, Munich, Germany, 2017, pp. 1160–1166.

[29] D. Schmitthenner, C. Sweeny, J. Du, and A. E. Martin, "The Effect of Stiff Foot Plate Length on Walking Gait Mechanics," *Journal of Biomechanical Engineering*, vol. 142, no. 9, p. 091012, Sep. 2020.